Using deeply trapped intermediates to map the cytochrome *c* folding landscape

F. Akif Tezcan, William M. Findley, Brian R. Crane, Scott A. Ross, Julia G. Lyubovitsky, Harry B. Gray*, and Jay R. Winkler*

Beckman Institute, California Institute of Technology, Pasadena, CA 91125

Contributed by Harry B. Gray, April 30, 2002

Replacement of iron with cobalt(III) selectively introduces a deep trap in the folding-energy landscape of the heme protein cytochrome *c*. Remarkably, neither the protein structure nor the folding thermodynamics is perturbed by this metal–ion substitution, as shown by data from spectroscopic and x-ray diffraction experiments. Through kinetics measurements, we have found parallel folding pathways involving several different misligated Co(III) species, and, as these folding intermediates persist for several hours under certain conditions, we have been able to elucidate fully their spectroscopic properties. The results, along with an analysis of the fluorescence energy-transfer kinetics during refolding, show that rapidly equilibrating populations of compact and extended polypeptide conformations are present until all molecules have reached the native structure. These measurements provide direct evidence that collapsed denatured structures are not substantially more stable than extended conformations of cytochrome *c*.

Significant advances in theory and experiment are producing an increasingly detailed description of how a polypeptide self-assembles into the native structure of a protein (1–11). Energy landscape theories (1, 12–15), in particular, have provided a framework for interpreting experimental investigations of protein folding kinetics. Despite this progress, many fundamental questions about protein folding dynamics remain to be answered.

Years of experimental work on the energetics and dynamics of self-assembly of cytochrome *c* (Cyt *c*) have failed to resolve whether unfolded polypeptides undergo global collapse to compact conformations on dilution or laser triggering to solution conditions that strongly favor the native structure (11, 16–26). Indeed, recent kinetics experiments suggest that comparable populations of compact and extended polypeptides are formed rapidly (<1 ms), and these two populations disappear in parallel as the protein folds (27, 28). To test this energy landscape model rigorously, we have isolated the structures that comprise the submillisecond (or "burst") phase by replacing the native iron center with cobalt(III) (29): because of very high ligand substitution barriers, the final step of cobalt(III)-Cyt *c* (Co-Cyt *c*) folding is well separated in time from all early events, and, in this kinetically stabilized system, the early folding intermediates can be examined carefully over a period of hours by an entire armamentarium of physical methods.

Materials and Methods

UV-visible and CD and fluorescence spectra were collected with Hewlett–Packard 8452A, Aviv (Lakewood, NJ) 62A DS, and Hitachi (Tokyo) F-4500 spectrometers, respectively. Fluorescence decay kinetics were measured as described previously (27). Horse, tuna, and yeast Co-Cyt were prepared according to established protocols (30, 31) with minor modifications. For the modification of yeast-Co-Cyt *c* with a dansyl fluorophore at Cys-102 (DNS-Co-Cyt *c*), FPLC-purified yeast Co-Cyt *c* was treated with excess 5-({[2-iodoacetyl)amino]ethyl}amino)-naphthalene-1-sulfonic acid (IAEDANS) (Molecular Probes), a thiol-specific derivative of the dansyl-fluorophore. DNS-Co-Cyt *c* was purified by using cation exchange FPLC and characterized by matrix-assisted laser desorption ionization (MALDI) mass spectroscopy (M_r = 13,008). Lysines in tuna or horse Co-Cyt *c* were converted into homoarginines (Har-Co-Cyt *c*) by using published protocols (32). Har-Co-Cyt *c* was purified by using cation exchange FPLC and characterized by MALDI mass spectroscopy [M_r = 13,159 (horse); 12,702 (tuna)].

Tuna Co-Cyt *c* crystals were grown at room temperature in sitting or hanging drops (≈50 mg/ml of protein) against a reservoir solution of 70–75% saturated $(NH_4)_2SO_4$, 0.75 M NaCl, and 0.1 M NaP_i (pH 6.5). X-ray diffraction data were collected at 100 K by using an R-Axis IV imaging plate area detector and monochromatized Cu-Kα radiation (1.54 Å) produced by a Rigaku (Tokyo) RU 200 rotating anode generator. The structure of Co-Cyt *c* was determined at 1.5-Å resolution by refinement of a model from isomorphous crystals (space group $P4_3$) of tuna heart Cyt *c* (PDB ID code, 3CYT) (33) against diffraction data (overall R_{sym} = 7.3%, overall $I/\sigma I$ = 16.4, completeness = 89.2%) by using DENZO (34). Rigid-body, simulated-annealing, positional, and thermal refinement with CNS (35), amid rounds of manual rebuilding, and water placement with XFIT (36) produced the final models (R_{cryst} = 18.3%, R_{free} = 22.0%, overall *B* factor = 13.9 Å^2). Bond and stereochemical constraints on Co-coordination were removed during refinement. The Ramachandran plot was calculated with PROCHECK (37).

^{1}H NMR spectra were acquired on a Varian Inova 600-MHz spectrometer equipped with a Nalorec Cryogenics (Martinez, CA) inverse probe with a self-shielded *z* gradient. Water suppression was achieved with presaturation during the relaxation delay. The spectra were processed with VNMR (Varian). All samples were prepared in 90:10 H_2O/D_2O and 50 mM NaP_i at pH 7. The final protein concentration in the samples was typically 0.3 mM or higher.

To extract distributions of donor–acceptor distances from the luminescence decay kinetics, we obtain $P(k)$ by inverting the discrete

$$I(t) = \sum_{k=k_o}^{\infty} P(k)\exp(-kt), \qquad [1]$$

Laplace transform that describes $I(t)$ (Eq. **1**) (38–40). In this expression, diffusion of the chromophores during the lifetime of the excited donor is neglected (40, 41). Transformation to a probability distribution over r [$P(r)$] is readily accomplished by using Eq. **2** (42). The value of k_o (9.6×10^7 s^{-1}) was obtained from

Abbreviations: Cyt *c*, cytochrome *c*; GuHCl, guanidine hydrochloride; FET, fluorescence energy transfer; DNS, dansyl fluorophore.

Data deposition: The atomic coordinates have been deposited in the Protein Data Bank, www.rcsb.org (access code 015902) (PDB ID code 1LFM).

*To whom reprint requests may be addressed. E-mail: hbgray@caltech.edu or winklerj@caltech.edu.

$$k = k_o + k_o\left(\frac{r_o}{r}\right)^6 \quad [2]$$

luminescence decay measurements with the DNS–cysteine model complex.

The difficulty in obtaining $P(r)$ arises in the first step because numerical inversion of $I(t)$ is extremely sensitive to noise (43). Regularization methods that impose additional constraints on the properties of $P(k)$ have been developed to stabilize inversion problems of this type. The simplest constraint that applies to the fluorescence energy transfer (FET) kinetics data is that $P(k) \geq 0$ ($\forall\ k$). Data were fit by using a MATLAB (Mathworks, Natick, MA) algorithm (LSQNONNEG) that minimized the sum of the squared deviations (X^2) between observed and calculated values of $I(t)$, subject to a non-negativity constraint. LSQNONNEG fitting produced narrow $P(k)$ distributions with relatively few nonzero components. Information theory suggests that the least biased solution to this inversion problem minimizes X^2 and maximizes the breadth of $P(k)$ (43). This regularization condition can be met by maximizing the Shannon–Jaynes entropy of the rate-constant distribution [$S = -\Sigma_k P(k) \ln\{P(k)\}$], implicitly requiring that $P(k) \geq 0$ ($\forall\ k$) (44). Maximum entropy (ME) fitting produced stable and reproducible numerical inversions of Eq. **1**. The balance between X^2 minimization and entropy maximization was determined by graphical L-curve analysis (45). The $P(k)$ distributions from ME fitting were broader than those obtained with LSQNNONEG fitting but exhibited comparable maxima. A straightforward coordinate transformation defined by Eq. **2** was used to recast the $P(k)$ results obtained from ME and LSQNONNEG fitting as probability distributions over r.

Results and Discussion

Cobalt-Substituted Cyt *c*. The absorption spectra of horse, tuna, and yeast Co-Cyt *c* are virtually identical (Soret maximum, 427 nm; Q-bands, 534, 568 nm), indicating that their heme environments are the same (30, 31). The far-UV CD spectrum of Co-Cyt *c* displays minima at 208 and 222 nm, characteristic of α-helical structures in the folded protein. The far-UV CD spectrum of guanidine hydrochloride (GuHCl) denatured Co-Cyt *c* suggests a random-coil conformation. Trp-59 fluorescence, fully quenched by energy transfer to the heme in the folded protein, has considerable intensity in the unfolded form, indicating loss of compact tertiary structure. The blue shifts in the absorption spectrum that accompany Co-Cyt *c* unfolding (Soret maximum, 422 nm; Q-bands, 530, 564 nm) reflect axial ligand substitution.

The folding free energies (ΔG_f) of horse, tuna, and yeast Co-Cyt *c* (9.9, 9.8, and 6.1 kcal/mol, respectively) determined by monitoring changes in far-UV CD and Soret absorption spectra in GuHCl solutions are comparable to those of the corresponding Fe(III)-protein (9.0, 9.4, and 4.6 kcal/mol) (46, 47). The folding thermodynamics accord with the crystal structure of tuna Co-Cyt *c* (1.5-Å resolution), which confirms that replacing Fe(III) with Co(III) does not disrupt the native protein fold [0.22-Å rms C_α displacements in Fe(III) and Co(III) proteins] (33, 48). The final model has good stereochemistry ($rmsd_{bond}$ = 0.018 Å, $rmsd_{angle}$ = 1.82°) (rmsd, rms deviation), with most residues (93.6%) in the favored and none in the disallowed regions of the Ramachandran plot. The His-18/Met-80 axial coordination of the metal is preserved in Co-Cyt *c*, although the metal–ligand bonds are slightly longer than those of the Fe(III)-protein ($d_{Met\text{-}80\text{-}Fe(III)}$ = 2.27 Å; $d_{Met\text{-}80\text{-}Co(III)}$ = 2.39; $d_{His\text{-}18\text{-}Fe(III)}$ = 2.00; $d_{His\text{-}18\text{-}Co(III)}$ = 2.03) (Fig. 1) (48). Metal–$N_{pyrrole}$ distances in Co-Cyt *c* are on average shorter than those in the native protein (M–N_A, N_B, N_C, N_D distances: M = Fe, 2.02, 2.03, 2.14, 2.11 Å; M = Co, 1.94, 1.95, 1.98, and 1.96 Å) (48).

Folding Kinetics. Both horse and tuna Co-Cyt *c* refold several orders of magnitude more slowly than the corresponding native protein; the observed kinetics are biphasic because of the presence of misligated unfolded protein populations (29) with different activation energies for ligand substitution (Fig. 2). In the horse protein, His-26 and His-33 are the likely axial ligands (49), and there is evidence that Lys side chains coordinate to Co(III) in the unfolded tuna protein, which lacks His-33 (29).

To investigate their involvement in Co-Cyt *c* folding, we converted the lysines in horse (19 total) and tuna (16 total) Co-Cyt *c* to homoarginine (Har) residues (32). Each Har has a single positive charge but, unlike lysines, should not coordinate to Co(III). Measurements of unfolding in GuHCl solutions demonstrate that Har-modified horse Co-Cyt *c* (Har-Co-Cyt *c*) is as stable as the unmodified protein. The biphasic folding

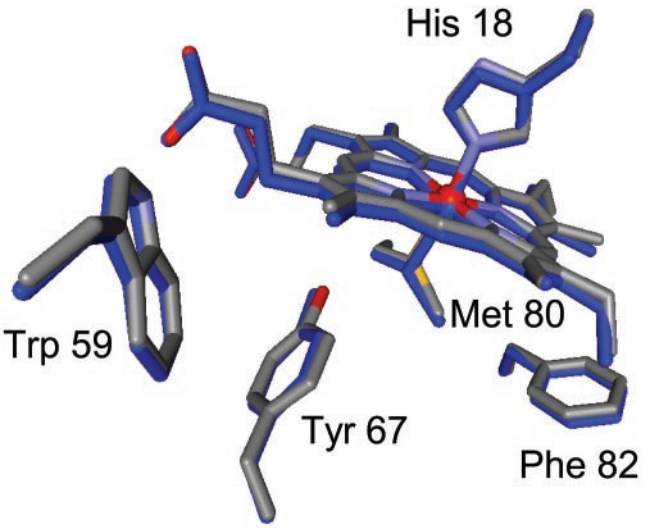

Fig. 1. Overlay of Fe-Cyt *c* and Co-Cyt *c* (blue) structures in the heme region.

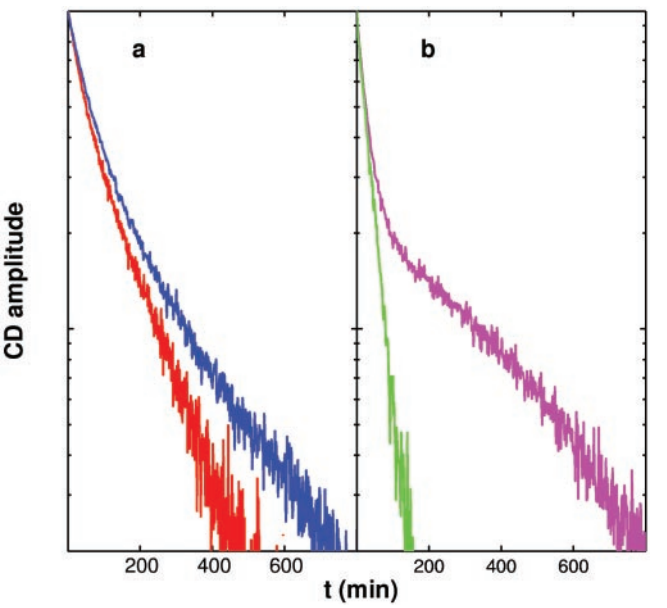

Fig. 2. Comparison of Co-Cyt *c* and Har-Co-Cyt *c* refolding kinetics measured by CD spectroscopy (228 nm). (*a*) Unmodified horse Co-Cyt *c* (red), horse Har-Co Cyt *c* (blue); (*b*) unmodified tuna Co-Cyt *c* (magenta), tuna Har-Co-Cyt *c* (green). Folding was initiated by manual dilution of a 4.0 M GuHCl solution to give a final denaturant concentration of 2.0 M at 25°C. The horse and tuna proteins were incubated in unfolding solutions for 10 min and 2 days, respectively.

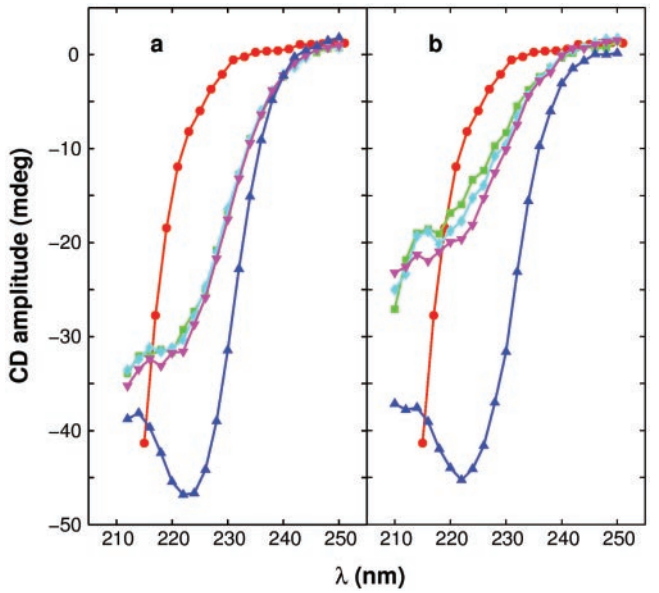

Fig. 3. Far-UV CD spectra of Co-Cyt *c* species observed during refolding in 0.4 M GuHCl at 7°C. (*a*) Horse Co-Cyt *c*: unfolded (red); *t* = 1 min (green); 10 min (cyan); 55 min (magenta); folded (blue) (*b*) tuna Co-Cyt *c*: unfolded (red); t = 1 min (green), 17 min (cyan); 48 min (magenta); folded (blue).

kinetics of this protein are quite similar to those of the unmodified species; the rates decrease slightly (≈1.5-fold) but exhibit similar relative amplitudes (Fig. 2*a*). On the other hand, tuna Har-Co-Cyt *c* folds in a single kinetics phase, even after incubation under denaturing conditions for 2 days before refolding (Fig. 2*b*). These findings confirm that lysines as well as histidines can coordinate to the metal center in denatured Cyt *c* at neutral pH.

Our analysis of the horse Co-Cyt *c* folding kinetics suggests that His-33 binds more tightly to the metal center than His-26 in the unfolded protein (29). The refolding phases associated with His-26- and His-33-misligated proteins exhibit comparable amplitudes after relatively short incubation periods in denaturant solution (5 min), indicating that the binding rates for the two histidines are similar (29). It follows from the equilibrium populations of unfolded protein {[Co(His 33)-Cyt *c*]:[Co(His 26)-Cyt *c*] ≈3:1 after 3 days of incubation in denaturing solution} that the dissociation rate for His-26 is three times greater than that for His-33, a finding that is in excellent agreement with the 3- to 4-fold faster folding rate for the His-26-misligated protein. We conclude from these results that folding is limited by His dissociation from Co(III), and that the weaker binding of His-26 to the metal center (relative to His-33) is due to unfavorable steric interactions associated with formation of a smaller loop (49).

Folding Intermediates. Pulsed H/D exchange NMR measurements at low [GuHCl] (pH 7) have revealed Cyt *c* folding intermediates in which the C- and N-terminal helices are docked together (17, 50). As expected, then, there is a large decrease in the far-UV CD amplitude (40% of total amplitude) immediately (≈5 s) after diluting horse Co-Cyt *c*/GuHCl solutions (to 0.8 M) (Fig. 3*a*). The helical intermediate persists at low temperature for several hours without significant change. An analogous tuna Co-Cyt *c* folding intermediate is observed under the same conditions, albeit with reduced helical content (Fig. 3*b*), because of replacement of His-33 with a lysine side chain. Several Lys residues are in the C- and N-terminal peptide regions and ligation to Co(III) by any of them would disfavor the formation and docking of terminal helices. The CD spectrum of the Co-Cyt *c* folding intermediate is similar to that reported recently for its Fe-protein analogue (51).

Unfolded Co-Cyt *c* displays a ^{1}H NMR spectrum characteristic of a random coil: the resonances are sharp and not dispersed (see Supporting Information on the PNAS web site, www.pnas.org). The upfield signals attributable to Met-80 side chain protons (52) in the spectrum of the folded protein are absent, consistent with His-misligation. Shortly (15 min) after the initiation of folding, when CD spectra indicate that helical intermediates are fully populated, resonances in the NMR spectrum are broadened and overlapped but remain negligibly dispersed. Such a spectrum indicates conformational exchange times comparable to the chemical shift time scale (on the order of milliseconds).

FET kinetics provide nanosecond-time-scale snapshots of donor–acceptor (D-A) distance distributions [$P(r)$] in rapidly equilibrating populations of folding intermediates (27). In our experiments, we examined FET kinetics from a DNS at Cys-102 to the Co(III)-porphyrin during yeast Co-Cyt *c* folding. The critical length (r_0) for the DNS/Co(III)-porphyrin energy-transfer pair is ≈40 Å, permitting determinations of DNS-Co(III) distances in the 12- to 60-Å range (42, 53). The DNS group displays intense fluorescence in GuHCl-denatured yeast Co-Cyt *c*, whereas its emission is significantly quenched by the Co(III)-porphyrin in the folded structure. Analysis of FET kinetics indicates that the folded protein ([GuHCl] ≈ 0.5 M) has a narrow D-A distance distribution centered at ≈27 Å; notably, the unfolding process is accompanied by a broadening of this distribution and appearance of extended conformations with $r_{D\text{-}A} > 50$ Å (Fig. 4).

A fraction of the DNS(Cys 102)-Co-Cyt *c* population collapses [average DNS-Co(III) distance of ≈30 Å] shortly after triggering folding by manual dilution of denaturant ($[GuHCl]_{final} \leq 0.5$ M) ($\tau \approx 2$ min) (Fig. 4). Interestingly, however, most of the molecules are still in extended conformations hours after initiating the refolding reaction; and, on an even longer time scale, both extended and compact conformations disappear as native structure forms. From these experiments, we have established that the time required to reach a DNS-Co(III) distance distribution characteristic of the native protein is >18 h.

Comparison of the FET results on Co-Cyt *c* with those obtained for Fe-Cyt *c* (27) is especially revealing. Immediately after triggering DNS(Cys 102)-Fe-Cyt *c* folding (≈1 ms), FET measurements reveal a bimodal distribution of DNS-Fe(III) distances: half of the protein molecules adopt compact structures, and the remainder are in extended conformations. As folding progresses, the compact and extended populations decrease in parallel and are replaced by folded protein. It is apparent, then, that similarly structured intermediates are populated in both the Fe(III) and Co(III) proteins. The key difference between the two is the refolding time scale: Fe-Cyt *c* evolves to the native structure in a few hundred milliseconds, whereas folding the Co(III)-protein requires several hours.

The combined spectroscopic probes of the "burst-phase" folding ensemble in Co-Cyt *c* shed new light on the nature of polypeptide structures that form immediately after dilution of denaturant solutions. CD spectra demonstrate that there are elements in the ensemble with some secondary structure, and the NMR spectra show clearly that those components are short-lived (milliseconds). Because the FET kinetics reveal populations of both compact and extended structures, it is likely that the compact structures give rise to the CD signal. The data strongly suggest that the compact and extended structures are in rapid equilibrium (20, 22, 54, 55). The Co-Cyt *c* folding data also are consistent with time-resolved small-angle x-ray scattering measurements that show that the Fe-Cyt *c* ensemble has a bimodal pair distribution function a few milliseconds after the initiation of folding (56).

The finding that compact and extended nonnative structures

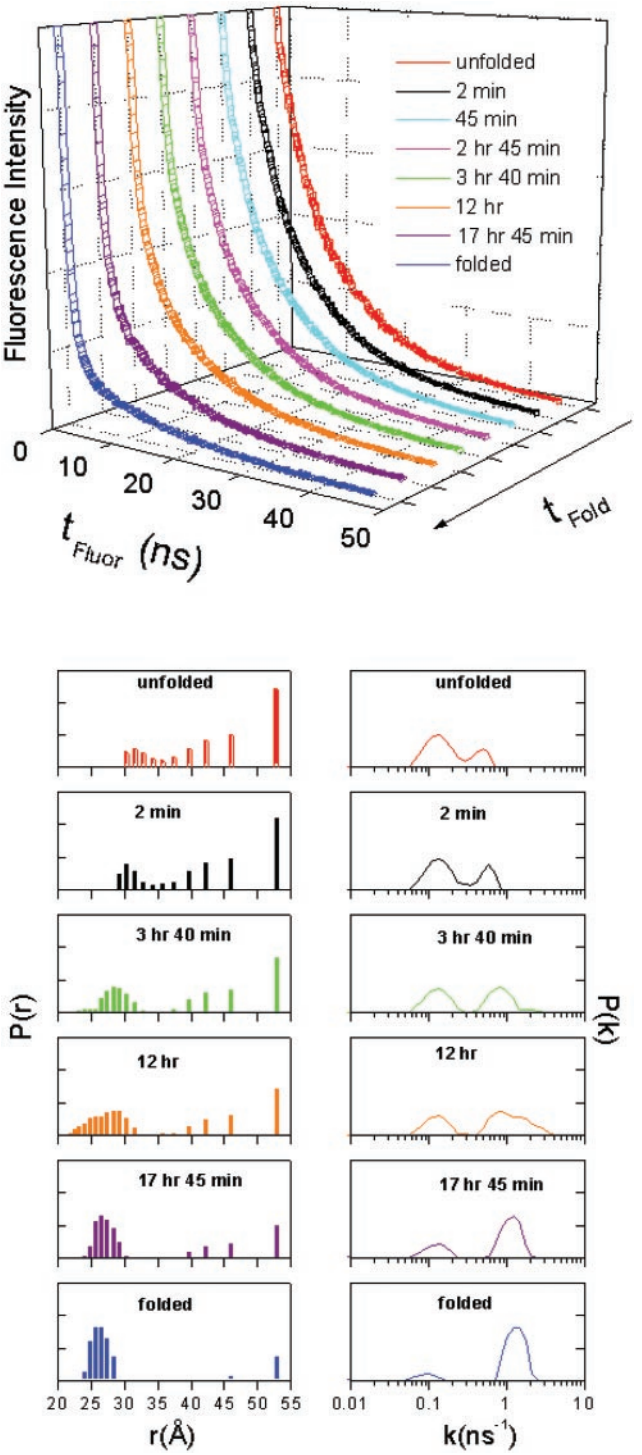

Fig. 4. (*Upper*) Luminescence decay kinetics of DNS(Cys 102)-Co-Cyt *c* measured at various times after initiating protein refolding by denaturant dilution {[GuHCl <0.5 M, pH 7}. (*Lower*) Distributions of excited-state decay rate constants [*P*(*k*)] and DNS-Co distances [*P*(*r*)] extracted from DNS luminescence decay kinetics at the specified folding times.

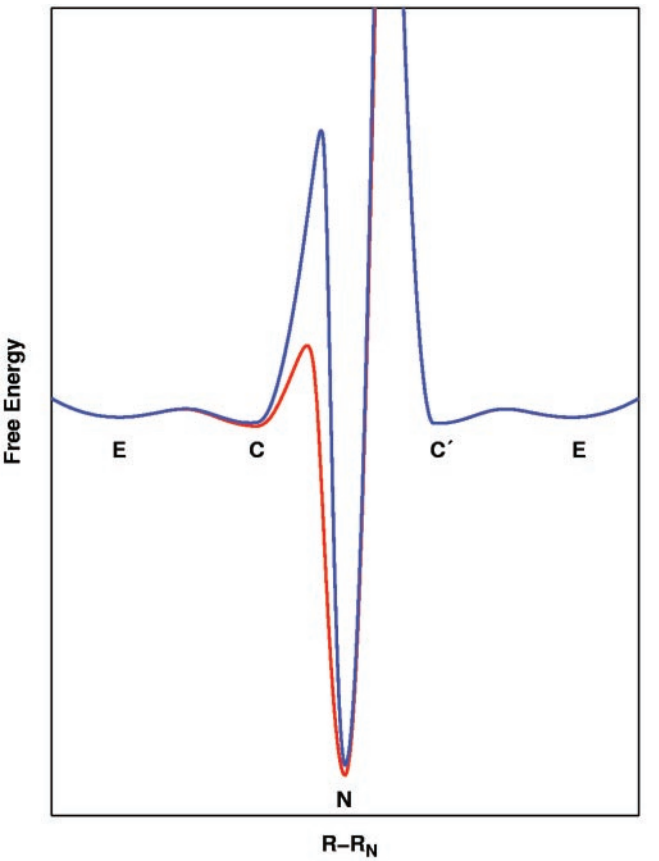

Fig. 5. Schematic representation of a two-dimensional cross section of the Cyt *c* folding energy landscape. The shallow energy minima correspond to nearly degenerate extended (**E**) and collapsed (**C**, **C**′) conformations. The collapsed structures on the left side of the global energy minimum (**C**) can surmount a ligand substitution barrier to reach the native (**N**) structure. This substitution barrier in Co-Cyt *c* (blue) is much higher than that of Fe-Cyt *c* (red). Collapsed peptides on the right side (**C**′) face a high topological barrier to formation of the native fold; this population must extend and collapse again to reach compact structures with lower barriers to folding.

are in rapid equilibrium immediately after denaturant dilution implies that the Cyt *c* folding energy landscape has a wide and relatively flat outer rim surrounding a narrow central funnel (Fig. 5). Although a fraction of the compact structures (**C**) can reach the native state (**N**) directly by ligand substitution (Fig. 5 *Left*), some polypeptides will collapse to conformations (**C**′) that cannot reach the final folded form, because of very high backbone-crossing barriers (Fig. 5 *Right*). These topologically frustrated molecules must return to the outer rim of the funnel to search the available conformation space for lower-barrier routes to the correctly folded product.

The possibility that global hydrophobic collapse is not an obligatory step in protein folding has been examined in computational experiments (57). Relative stabilities of collapsed and extended conformations were suggested to correlate with the properties of the primary sequences and overall stability of the folded protein: more hydrophobic and less optimized sequences favored formation of collapsed intermediates, whereas extended structures evolved directly to the native fold in less hydrophobic and strongly optimized sequences (57). The sequence and stability of Cyt *c* appear to place it between these two limits: in this case, extended and collapsed structures are degenerate, and nearly all of the folding free energy is released when the compact conformations convert to the native fold. The relative instability of collapsed nonnative structures not only prevents formation of misfolded structures during the self-assembly process but also reduces the probability that the native protein will transiently adopt an incorrect conformation.

This research was supported by the National Science Foundation (MCB 9974477; DBI 9876443) and the Arnold and Mabel Beckman Foundation.

1. Onuchic, J. N., Nymeyer, H., Garcia, A. E., Chahine, J. & Socci, N. D. (2000) *Adv. Protein Chem.* **53,** 87–152.
2. Portman, J. J., Takada, S. & Wolynes, P. G. (2001) *J. Chem. Phys.* **114,** 5069–5081.
3. Portman, J. J., Takada, S. & Wolynes, P. G. (2001) *J. Chem. Phys.* **114,** 5082–5096.
4. Özkan, S. B., Bahar, I. & Dill, K. A. (2001) *Nat. Struct. Biol.* **8,** 765–769.
5. Mirny, L. & Shakhnovich, E. I. (2001) *Annu. Rev. Biophys. Biomol. Struct.* **30,** 361–396.
6. Kazmirski, S. L., Wong, K. B., Freund, S. M. V., Tan, Y. J., Fersht, A. R. & Daggett, V. (2001) *Proc. Natl. Acad. Sci. USA* **98,** 4349–4354.
7. Wong, K. B., Clarke, J., Bond, C. J., Neira, J. L., Freund, S. M. V., Fersht, A. R. & Daggett, V. (2000) *J. Mol. Biol.* **296,** 1257–1282.
8. Eaton, W. A., Munoz, V., Hagen, S. J., Jas, G. S., Lapidus, L. J., Henry, E. R. & Hofrichter, J. (2000) *Annu. Rev. Biophys. Biomol. Struct.* **29,** 327–359.
9. Kuwata, K., Shastry, R., Cheng, H., Hishino, M., Batt, C. A., Goto, Y. & Roder, H. (2001) *Nat. Struct. Biol.* **8,** 151–155.
10. Jager, M., Nguyen, H., Crane, J. C., Kelly, J. W. & Gruebele, M. (2001) *J. Mol. Biol.* **311,** 373–393.
11. Englander, S. W., Sosnick, T. R., Mayne, L. C., Shtilerman, M., Qi, P. X. & Bai, Y. (1998) *Acc. Chem. Res.* **31,** 737–744.
12. Bryngelson, J. D., Onuchic, J. N. & Wolynes, P. G. (1995) *Proteins Struct. Funct. Genet.* **21,** 167–195.
13. Dill, K. A. & Chan, H. S. (1997) *Nat. Struct. Biol.* **4,** 10–19.
14. Onuchic, J. N., Lutheyschulten, Z. & Wolynes, P. G. (1997) *Annu. Rev. Phys. Chem.* **48,** 545–600.
15. Wolynes, P. G. (1996) *Proc. Natl. Acad. Sci. USA* **93,** 14249–14255.
16. Bai, Y., Sosnick, T. R., Mayne, L. & Englander, S. W. (1995) *Science* **269,** 192–197.
17. Elöve, G., Bhuyan, A. K. & Roder, H. (1994) *Biochemistry* **33,** 6925–6935.
18. Eaton, W. A., Thompson, P. A., Chan, C. K., Hagen, S. J. & Hofrichter, J. (1996) *Structure (London)* **4,** 1133–1139.
19. Pollack, L., Tate, M. W., Darnton, N. C., Knight, J. B., Gruner, S. M., Eaton, W. A. & Austen, R. H. (1999) *Proc. Natl. Acad. Sci. USA* **96,** 10115–10117.
20. Hagen, S. J. & Eaton, W. A. (2000) *J. Mol. Biol.* **301,** 1019–1027.
21. Shastry, M. C. R., Sauder, J. M. & Roder, H. (1998) *Acc. Chem. Res.* **31,** 717–725.
22. Shastry, M. C. R. & Roder, H. (1998) *Nat. Struct. Biol.* **5,** 385–392.
23. Pierce, M. M. & Nall, B. T. (1997) *Protein Sci.* **6,** 618–627.
24. Pascher, T., Chesick, J. P., Winkler, J. R. & Gray, H. B. (1996) *Science* **271,** 1558–1560.
25. Chan, C. K., Hofrichter, J. & Eaton, W. A. (1996) *Science* **274,** 628–629.
26. Winkler, J. R. & Gray, H. B. (1996) *Science* **274,** 629–631.
27. Lyubovitsky, J. G., Gray, H. B. & Winkler, J. R. (2002) *J. Am. Chem. Soc.,* **124,** 5481–5485.
28. Lee, J. C., Chang, I.-J., Gray, H. B. & Winkler, J. R. (2002) *J. Mol. Biol.,* in press.
29. Tezcan, F. A., Winkler, J. R. & Gray, H. B. (1999) *J. Am. Chem. Soc.* **121,** 11918–11919.
30. Dickinson, L. C. & Chien, J. C. W. (1975) *Biochemistry* **14,** 3526–3534.
31. Dickinson, L. C. & Chien, J. C. W. (1975) *Biochemistry* **14,** 3534–3541.
32. Russell, B. S., Melenkivitz, R. & Bren, K. L. (2000) *Proc. Natl. Acad. Sci. USA* **97,** 8312–8317.
33. Takano, T. & Dickerson, R. E. (1980) *Proc. Natl. Acad. Sci. USA* **77,** 6371–6375.
34. Otwinowski, Z. & Minor, W. (1997) *Methods Enzymol.* **276,** 307–326.
35. Brünger, A. T., Adams, P. D., Clore, G. M., DeLano, W. L., Gros, P., Grosse-Kunstleve, R. W., Jiang, J. S., Kuszewski, J., Nilges, M., Pannu, N. S., *et al.* (1998) *Acta Crystallogr. D* **54,** 905–921.
36. McRee, D. (1992) *J. Mol. Graphics* **10,** 44–46.
37. Laskowski, R. A., Macarthur, M. W., Moss, D. S. & Thornton, J. M. (1993) *J. Appl. Crystallogr.* **26,** 283–291.
38. Beecham, J. M. & Haas, E. (1989) *Biophys. J.* **55,** 1225–1236.
39. Beals, J. M., Haas, E., Krausz, S. & Scheraga, H. A. (1991) *Biochemistry* **30,** 7680–7692.
40. Navon, A., Ittah, V., Landsman, P., Scheraga, H. A. & Haas, E. (2001) *Biochemistry* **40,** 105–118.
41. Hagen, S. J., Hofrichter, J. & Eaton, W. A. (1997) *J. Phys. Chem. B* **101,** 2352–2365.
42. Förster, T. (1948) *Ann. Phys. (Leipzig)* **2,** 55–75.
43. Istratov, A. D. & Vyvenko, O. F. (1999) *Rev. Sci. Instrum.* **70,** 1233–1257.
44. Livesey, A. K. & Brochon, J. C. (1987) *Biophys. J.* **52,** 693–706.
45. Lawson, C. L. & Hanson, R. J. (1974) *Solving Least Squares Problems* (Prentice–Hall, Englewood Cliffs, NJ).
46. Mines, G. A., Pascher, T., Lee, S. C., Winkler, J. R. & Gray, H. B. (1996) *Chem. Biol.* **3,** 491–497.
47. Tezcan, F. A. (2001) Ph.D. thesis (California Institute of Technology, Pasadena), p. 164.
48. Swanson, R., Trus, B. L., Mandel, N., Mandel, G., Kallai, O. B. & Dickerson, R. E. (1977) *J. Biol. Chem.* **252,** 759–775.
49. Colón, W., Wakem, L. P., Sherman, F. & Roder, H. (1997) *Biochemistry* **36,** 12535–12541.
50. Roder, H., Elöve, G. A. & Englander, S. W. (1988) *Nature (London)* **335,** 700–704.
51. Akiyama, S., Takahashi, S., Ishimori, K. & Morishima, I. (2000) *Nat. Struct. Biol.* **7,** 514–520.
52. Moore, G. R., Williams, R. J. P., Chien, J. C. W. & Dickinson, L. C. (1980) *J. Inorg. Biochem.* **12,** 1–15.
53. Duus, J. Ø., Meldal, M. & Winkler, J. R. (1998) *J. Phys. Chem. B* **102,** 6413–6418.
54. Pande, V. S. & Rokshar, D. S. (1998) *Proc. Natl. Acad. Sci. USA* **95,** 1490–1494.
55. Eaton, W. A. (1999) *Proc. Natl. Acad. Sci. USA* **96,** 5897–5899.
56. Akiyama, S., Takahashi, S., Kimura, T., Ishimori, K., Morishima, I., Nishikawa, Y. & Fujisawa, T. (2002) *Proc. Natl. Acad. Sci. USA* **99,** 1329–1334.
57. Gutin, A. M., Abkevich, V. I. & Shakhnovich, E. I. (1995) *Biochemistry* **34,** 3066–3076.